Rapid μm ITO Electrode Patterning by Laser-direct Writing Using a Modest Commercial Fibre Laser Scriber

Ting-Wei Guo[1,2], Wei-Chen Kao[1], and Ji-Yen Cheng [*1,2,3,4]

[1]- *Research Center for Applied Sciences, Academia Sinica, Taipei, Taiwan*
[2]- *Institute of Biophotonics, National Yang Ming Chiao Tung University, Taipei, Taiwan*
[3]- *Department of Mechanical and Mechatronic Engineering, National Taiwan Ocean University, Keelung, Taiwan*
[4]- *College of Engineering, Chang Gung University, Taoyuan, Taiwan*
[*]*Corresponding author's e-mail:jycheng@gate.sinica.edu.tw*

This work presented a rapid method for determining indium tin oxide (ITO) ablation threshold. The method relies on the conduction property of the ITO film and measured the resistance changes of an ITO test strip after the laser ablation. The method can rapidly measure the lowest laser fluence that produced the resistance increase of the test strip. The method is simpler compared to the typical method that requires the microscopic measurement of laser ablated spot sizes. We determined the ITO laser ablation parameters for three types of ITO slides and prepared ITO conducting electrodes with width smaller than 10 μm. The result demonstrated the effectiveness and flexibility of a modest and inexpensive NIR laser scriber for ITO microelectrode writing.

DOI: 10.2961/jlmn.2023.02.2002
Keywords: ITO, laser direct-writing, threshold, micro electrode, fiber laser, galvanometer scanning

1. Introduction

Indium-tin oxide (ITO) is a transparent conductive oxide material that is widely used in flat-panel display [1] and has also been tested for sensing applications such as microfluidic flow sensor[2] and extended FET pH sensor [3].

Laser micromachining of Indium tin oxide-coated glass (ITO thin-film coated-glass) is a precise and versatile technique that offers a wide range of applications in various industries. By using a laser to selectively remove or modify the ITO coating on glass substrates, the creation of intricate patterns, microstructures, or microchannels with high precision and accuracy can be achieved. The ITO coating, known for its excellent electrical conductivity and optical transparency, makes it ideal for applications such as touchscreens, flat-panel displays, photovoltaics, and smart windows. Laser micromachining of ITO-coated glass provides a flexible, cost-effective and efficient method for fabricating complex microdevices and functional structures, enabling possibilities for advanced electronics, optoelectronics, and microfluidics.

Laser micromachining of the ITO thin film has been realized using nanosecond (ns) pulse lasers [4-9], picosecond (ps) pulse lasers [10-12] and femtosecond (fs) pulse lasers [7, 13, 14]. Tanaka et. al has tried the ITO thin film removal using 50 ns laser pulses with wavelength from UV to NIR including 262 nm, 349 nm, 524, and 1047 nm [8]. All wavelengths results in ITO thin film ablation. They have also found the laser ablation process under helium (He) gas environment provides the ITO removal with least debris generation. Tanaka et. al. has also demonstrated ITO film removal using 30 fs 800 nm laser pulses [14]. The use of the ultrashort pulses solves the heat affected zone (HAZ) problem and results in the least molten material, micro crack, and debris formation under atmosphere processing.

Indirect ITO removal using laser-induced-backside-wet-etching (LIBWE) has also been reported using nanosecond visible laser pulses [2]. ITO patterning using laser direct-write followed by acidic etching has been achieved using infrared ns fiber laser [15], femtosecond lasers [13], and 355 nm UV laser[16]. Ablation of ITO coated on polycarbonate, cyclic olefin copolymer, and glass using 1064 nm Nd:YAG laser has also been compared [6].

Previous studies have reported that laser ablation of silver (Ag) in liquid has a threshold of 0.6 J/cm^2 [17]. Nanosecond laser ablation of single crystalline silicon surface has threshold of 0.8 J/cm^2 [18]. For picosecond laser ablation of gallium nitride (GaN) film has threshold of 0.13 J/cm^2 [19]. As can be seen in the literature, ablation threshold is the crucial factor for material processing. Ablation threshold is also one of the major laser parameters for achieving clean ITO layer removal so that isolated conduction lines or electrodes can be obtained. Typically, the threshold is obtained by monitoring the minimal laser fluence that results in damage on the ITO film, while the damage is observed by microscopic images. For example, the ablation spot sizes caused by increasing laser fluences are measured and the fluence that produces the smallest diameter is calculated to be the threshold fluence[20]. The method relies on repetitive microscopic observation and has significant measurement error.

This work utilizes a commercial ns fiber laser for rapid scanning ablation of ITO thin film coated on glass for the fabrication of micrometer-sized electrodes. A rapid method based on measuring ITO resistance change was used to determine the ablation threshold, and that the result was compared to that obtained by measuring ablation spot sizes [20]. The surface quality obtained by the rapid scanning fabrication process was also measured and compared to those obtained by other types lasers.

2. Materials and Methods

The ITO-coated slides with three different square resistances (5 Ω/□, 50 Ω/□, and 90 Ω/□) were purchased from SCIKET Taiwan (Cat. No. SGAST0001-CUS-160933). The nominal ITO film thicknesses were 220±30 nm, 40±5 nm, and 23±5 nm, respectively. A commercial grade fiber laser scriber system (Synmao Taiwan, Model RK-10) is used for the ITO surface scribing. The maximal laser output power is 10 Watt. The laser wavelength is 1064 nm. The laser pulse duration is ~ 150 ns, which was measured by a high-speed (1 ns rise time) photodiode (Thorlabs DET-210) terminated with a 50 Ω load. The pulse repetition rate was set at 30 kHz. The laser output is scanned by the galvanometer mirror scanner (galvo scanner for short) equipped with the laser system and focused using a theta lens with focal length of 300 mm. A scanning area of 100 mm x 100 mm is provided by the system shown in **Fig. 1** (a).

The ITO ablation threshold was determined by using two methods. The first method measured the ITO resistance change and the obtained fluence threshold is denoted as ThR. The second method measured the ablated spot size and the obtained threshold is denoted as Thδ. For obtaining ThR, a test strip of ITO (denoted as the "test strip" below) was prepared (Fig. 1(b)) using a laser power that ensured the electrical isolation of the strip (25 mm long x 2.5 mm wide) from the surrounding ITO layer. A single laser line ablation (denoted as the "test stroke" below) was then applied to the center of the test strip and the resistance of the strip was measured using a multimeter (Fluke, model 289). An increase in the resistance indicated the removal of the ITO conductive film. The ablation threshold was then obtained by observing the minimal fluence that resulted in the resistance increase. The beam scanning speed for this method was set to 400 mm/sec.

The second method for obtaining ablation threshold is by measuring the ablated spot size under different fluence according to the equation [20]:

$$\delta^2 = 4\omega_0^2 [\ln (E/E_{th})] \quad (1)$$

, where δ is the ablated diameter measured observed under a laser scanning microscope (Keyence, VK-9700), ω_0 is the $1/e^2$ laser focus radius [20] [21], E is the pulse energy causing the corresponding δ , and E_{th} is the threshold pulse energy.

The pulse energy is related to the laser power, W, by the following equation:

$$E = W/(fA) \quad (2)$$

, where f is the laser pulse repetition rate and $A = \pi \omega_0^2$ is the laser spot area.

By plotting δ^2 produced by different pulse powers, a linear plot was obtained and the slope was used for calculating the laser focus radius (ω_0) and the corresponding effective area. For this method, a rapid scanning speed of 1300 mm/sec was used so that the spot size ablated by individual pulses could be measured. The threshold power was determined by the X-axis intercept of the δ^2-ln(W) plot and used to calculate the threshold fluence. The obtained threshold by this method is denoted as Thδ. The procedure is detailed in Sec. 3.1.

During a line-scanning ablation on the ITO surface, consecutive laser pulses overlapped and formed a line (Fig. 1 (c)). The overlapping ratio (OR) of the consecutive pulses is calculated by the laser spot diameter (D = 2 ω_0) and the center-to-center distance (dn) using the equation:

$$OR = [(D - dn)/D] \times 100\ \% \quad (3)$$

, where dn is the spot-to-spot distance, as calculated by dividing the beam scanning speed by the pulse repletion rate. The laser beam scanning speeds of 100 mm/sec to 900 mm/sec were used for obtaining corresponding OR of about 90 % to 30 %.

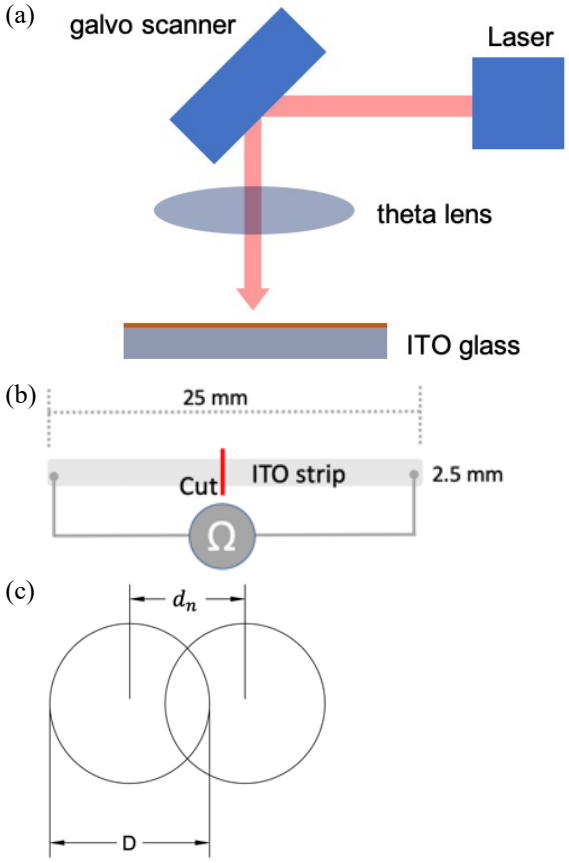

Fig. 1 (a) The schematic drawing of the laser scribing system. (b) The pattern of the ITO test strip used for measuring the ablation threshold by resistance changes (ThR). The red line indicates the test stroke. (c) The spot-to-spot distance (dn) and the laser focus spot diameter used for the calculation of overlapping ration (OR).

The ablated spot diameter, the surface roughness, and the cross-sectional profile of the scribed ITO was measured using a laser scanning profiler (Keyence, VK-9700). The roughness was also observed using a scanning electron microscope (SEM, FEI, Model FEI200). The surface ITO removal was measured using an energy dispersive X-ray spectroscopy (EDS) analysis module (Model X-MAX150) equipped on the SEM. For the SEM observation, the sample was coated with 10 nm Au. For the EDS analysis, the samples were not coated. Indium (In) signal intensity was used to identify the ITO thin film layer above the glass layer.

3. Results and Discussion

We first determined the laser ablation thresholds, ThR, and Thδ, and the laser focus spot diameter, *D*. Then the surface quality after the laser ablation were observed.

3.1 Ablation thresholds

The ablation thresholds were determined using the two methods. The first one is by measuring the ITO film resistance change and determines the ThR.

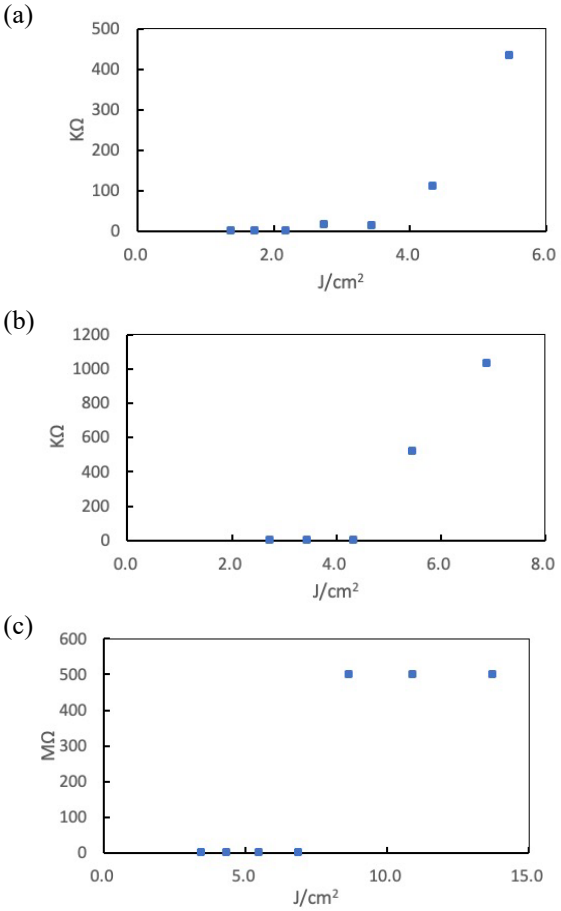

Fig. 2 The resistance changes of the ITO test strip after the test stroke ablation at different fluences. (a) 5 Ω/□. (b) 50 Ω/□. (c) 90 Ω/□. The beam scanning speed was 400 mm/sec.

Fig. 2 shows the resistance changes of the ITO test strips (Fig. 1(b)) after the test stroke ablation on three types of ITO glass. The smallest fluence that caused the increase of the test strip resistance was considered as the threshold fluence, ThR. The values for the three types of ITO slide are summarized in Table 1.

The second method used the ablated diameter for determining the threshold, Thδ, and the laser focus spot diameter (*D*). Fig. 3 shows the plot of δ^2 at different laser power, *W*, on the ITO slides. According the eq.(1), the slope obtained by the linear fitting of the plot was used to calculate the laser focus radius, ω_0, and the corresponding diameter, *D*, was calculated to be 43 μm. The laser diameter, *D*, was used to calculate the laser spot area $A_{1/e2}$ and then the effective area A_{eff}, which equals (1/2)x($A_{1/e2}$), was obtained [22]. The linear fitting was also used to calculate the extrapolating intercept with the X-axis, which corresponds to the power that produced the smallest ablated diameter. The laser fluence at the intercept was divided by Aeff to obtain the threshold, Thδ, for the three types of ITO slide used. The values are summarized in Table 1.

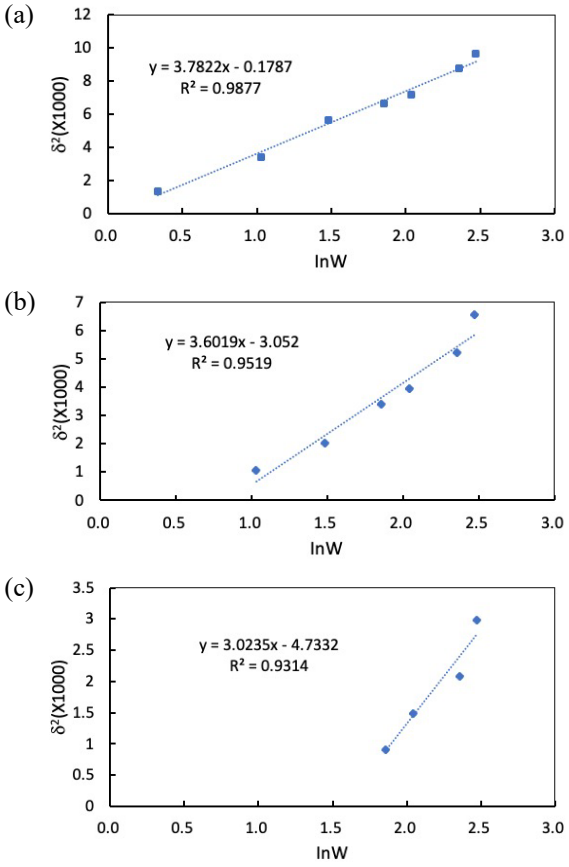

Fig. 3 The plot of the square of the ablated diameter, δ^2, at different laser powers. (a) 5 Ω/□. (b) 50 Ω/□. (c) 90 Ω/□. The beam scanning speed was set at 1300 mm/sec. The insets show the equation and regression coefficient, R^2, of the linear fitting lines.

Table 1 compares the ThR and Thδ values for the three types of ITO slides used in this study. It is found that the ITO slides with lower square resistance shows lower threshold. For the two determination methods, the trend is the same. The trend is in accordance to the study that uses 1064 nm ps laser pulses for ITO ablation [21], by which thinner ITO film requires higher ablation threshold. The phenomenon can be attributed to the incubation effect observed by using fs laser pulses for ITO thin film ablation. [23]

Park et. al. [1] have found that, using fs 810 nm laser pulses, the ablation threshold of ITO thin film is 0.07 J/cm^2 while that of glass substrate is about 1.2–1.6 J/cm^2. Yavas et. al. [9] have used 1047 nm 15 ns laser pulses on ITO patterning and have found the threshold to be 18 J/cm^2, which is larger than the values obtained by our work. The discrepancy on the threshold values may be caused by the following reasons.

As has been indicated by Yavas et. al. the ITO film absorbs about 20% of the incoming IR light and the glass substrate is completely transparent but could act as a thermal conductance barrier. The relatively long pulse duration (150 ns) used in this work may enhance the incubation effect.

Another reason that may have caused the difference of the ablation threshold values is the errors in measuring the laser ablated spot size. As can be seen in Fig. 3, the data scattering on the ablated spot size is apparent. Moreover, the calculation of Thδ required the measurement of spot sizes under a microscope, which is more time consuming compared to the resistance change measurement. The method of ThR measurement could provide the threshold information in a simpler way than that for Thδ.

Table 1 The ablation threshold for the three types of ITO glass substrates using the two different determination methods.

		5 Ω/□	50 Ω/□	90 Ω/□
Threshold (J/cm²)	ThR	2.5	4.9	7.8
	Thδ	2.4	5.0	7.8

3.2 Surface quality

The surface quality of the ablated substrates was observed by a laser scanning profiler and an SEM.

Fig. 4 shows the optical images of the ITO glass surface ablated with different laser fluences. Figures 4(a), 4(c), and 4(e) show the surfaces ablated with fluences slightly above the threshold. Figures 4 (b), 4(d), and 4(f) show the surfaces ablated with fluences that ensured total ITO film removal.

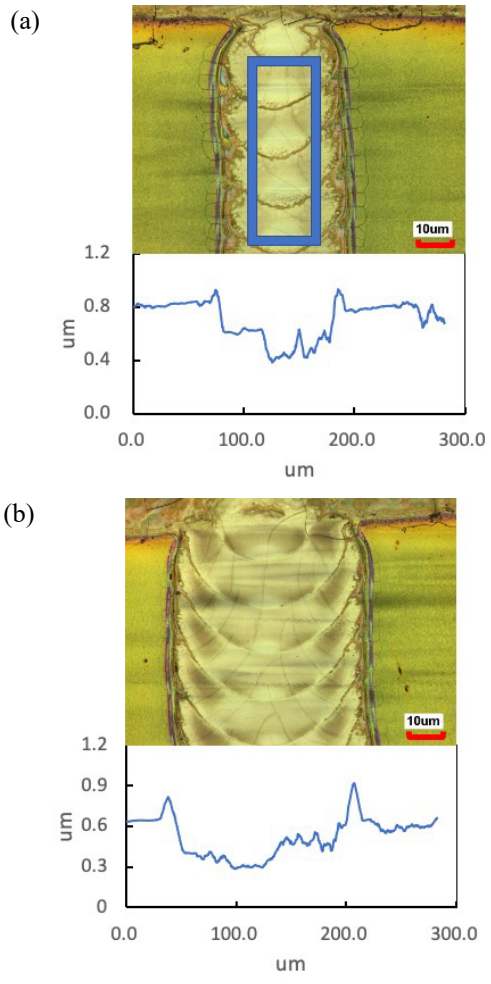

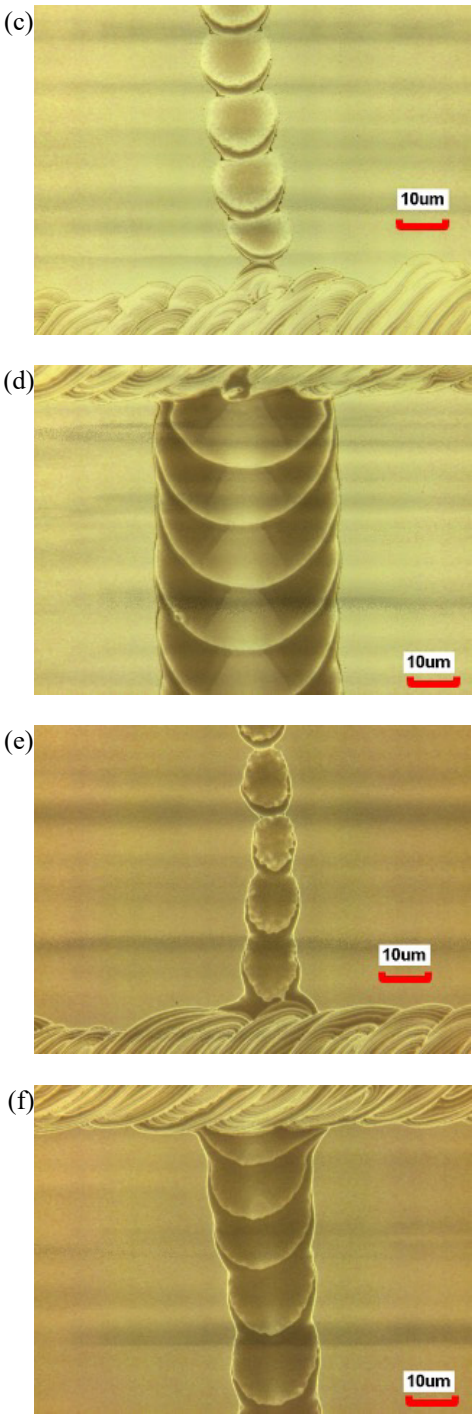

Fig. 4 The surface quality ((a) to ((f)) and the cross-sectional profile ((a) and (b)) of the laser ablated regions on three types of ITO slides observed by the VK laser scanning profiler. (a) 5 Ω/□, fluence 2.7 J/cm². The inset marks the area where the roughness, Ra, was measured. (b) 5 Ω/□, fluence 5.5 J/cm². (c) 50 Ω/□, fluence 4.3 J/cm². (d) 50 Ω/□, fluence 6.9 J/cm². (e) 90 Ω/□, fluence 6.9 J/cm². (f) 90 Ω/□, fluence 13.7 J/cm². The horizontal ablation line is the edge of the ITO test strips. The vertical ablation beam scanning speed is 400 mm/sec.

In the images for the 5Ω/□ slides (Figures 4(a) and 4(b)), clear cracks were observed on the ITO layer along the ablation edge. However, the cracks were not necessarily on the surface but may be latent in the underlying glass layer (please see the SEM result below). The cracks were observed for both the low and the high fluences. Since the ablation is induced by the absorption of the 1064 nm laser energy by the ITO film, the cracks are apparently the heat-affected-zone (HAZ). However, no cracks of ITO film were observed for the 50 Ω/□ slides and the 90 Ω/□ slides at the fluences higher than those used for the 5 Ω/□ slides, which has a relatively thick (~220 nm) ITO layer. The results suggest that the HAZ was significant for substrate with thick ITO-film, which absorbed and accumulated the incident laser energy. For the 50 Ω/□ slides and the 90 Ω/□ slides, the relatively thin ITO layers assisted in the heat dissipation during the ablation and hence no cracking on the ITO layer was observed.

The cross-sectional profile shown in Figures 4(a) and 4(b) also indicated clear bump at the ablation edge. Also, higher fluence resulted in higher bump height. This characteristic is discussed in the Table 2 and Table 3 below.

It is also noticed that no cracks were observed on the underlying glass layer at the ablated region on the 50 Ω/□ slides and the 90 Ω/□ slides where ITO was totally removed (Figures 4 (c), (d), (e), and (f)). This is in accordance with the speculation that the thickness of the ITO layer is the major parameter causing the formation of the HAZ.

Fig. 5 shows the SEM photographs of 5Ω/□ slides and the 50Ω/□ slides, corresponding to the ablation conditions in Fig. 4. In Figures 5(a) and 5(b), no crack was observed on the surface of the ITO film and the underlying glass layer. This is seemingly contradictory to the results shown in Fig. 4(a) and 4(b), in which clear cracks were observed. However, the SEM only reveals the surface quality while the optical profiler observes both the transparent ITO film and the underlying glass layer. It is likely that the cracks observed in Figures 4(a) and (b) are latent cracks of the underlying glass but not of the surface ITO film. The speculation is in accordance with the fact that no crack was optically observed on the 50 Ω/□ slides and the 90 Ω/□ (Figures 4(c), 4(d), 4(e), and 4(f)) because they both have thinner ITO and hence faster heat dissipation than that on the 5 Ω/□ slides.

Fig. 5 SEM photographs of the laser ablated region on different slides using different laser fluences. The ablation beam scanning speed is 400 mm/sec. (a) 5 Ω/□, 2.7 J/cm^2. (b) 5 Ω/□, 5.5 J/cm^2. (c) 50 Ω/□, 4.3 J/cm^2. (d) 50 Ω/□, 6.9 J/cm^2. The magenta rectangles in (c) and (d) mark the region used for EDS analysis below.

The surface quality under the different ablation conditions were further quantified by the laser scanning profiler. The surface roughness, Ra, measured by the profiler is listed in Table 2. The results showed that the 5 Ω/□ slides had the highest surface roughness after the ablation, while the other two types of ITO slides had similar Ra, which is close to the roughness of the pristine smooth ITO surface.

We have tested the ablation using OR from 30 % to 90 %. The result indicated that the accumulation of the laser pulses has no significant effect on the surface roughness Ra and the data is therefore not shown here. The result further supports the previous suggestion that the ITO layer thickness is the major parameter affecting the surface quality after the ablation.

Table 2 The surface roughness, Ra, of the regions ablated using different laser fluences.

Ra (fluence J/cm²)		**5 Ω/□**	**50 Ω/□**	**90 Ω/□**
	Near threshold	100 nm (2.7)	40 nm (4.3)	60 nm (6.9)
	Total removal	100 nm (5.5)	50 nm (6.9)	50 nm (13.7)

The result in Table 2 also indicates that the near-threshold fluence produces similar roughness and therefore similar quality to that by fluences that resulted in total ITO removal.

We further examined the height of the bump along the ablation edge, together with the ablation depth, as shown in Table 3. For the 5 Ω/□ slides, the bump height using the higher fluence resulted in higher bump. However, for 50 Ω/□ slides and 90 Ω/□ slides, the fluences did not clearly affect the bump height irrespective of the removal depth. In summary, better ablation quality were obtained for slides with thinner ITO film, such as the 50 Ω/□ slides and 90 Ω/□ slides. The bump height (~100 nm) for the 5 Ω/□ slides obtained in this work is similar to that in previous works by direct ablation [9, 23].

Table 3 The edge bump height along the ablation edge and the depth of ablation using different laser fluences.

		5Ω/□	**50 Ω/□**	**90 Ω/□**
Bump /Depth	Near threshold	130 nm /340 nm	29 nm /11nm	8 nm /7 nm
	Total removal	273 nm /339 nm	20 nm /48 nm	6 nm /14 nm

3.3 ITO removal observed by EDS

The removal of the ITO layer by the laser ablation was examined using EDS. We measured the distribution of Indium (In) at the laser ablated region and used it as an indicator of the conducting layer.

Fig. 6 shows the distribution of the representative element, In, of the ITO layer ablated using the conditions corresponding to those in Fig. 4. Fig. 6 shows that, on the 5 Ω/□ slides, the region with partial ITO removal (6(a)) shows clear In residue while the remaining In on the total removal region (6(b)) is apparently weaker. The similar difference is observed on the 50 Ω/□ slides.

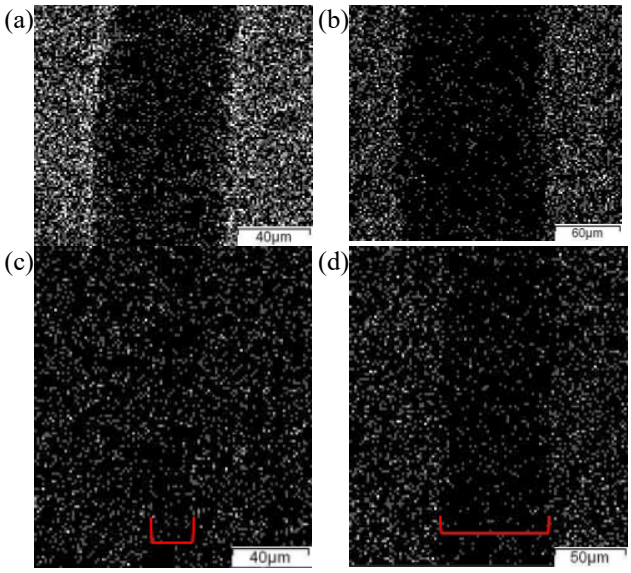

Fig. 6 The distribution of In at the laser ablated region. The laser beam scanning speed is 400 mm mm/sec. (a) 5 Ω/□, 2.7 J/cm^2. (b) 5 Ω/□, 5.5 J/cm^2. (c) 50 Ω/□, 4.3 J/cm^2. (d) 50 Ω/□, 6.9 J/cm^2. The red parenthesis denotes the region of the ablated region in (c) and (d).

We further quantify the element ratio measured by EDS. Fig. 7 shows the composition of elements on the 50 Ω/□ slides before and after the ablation. The result clearly shows the partial ITO removal (7(b)). The result supports the rational of our threshold determining method based on resistance change. The partial removal caused by the laser ablation reduced the electrical conduction. The change can be measured before total removal is achieved. We conclude that the resistance-change method is more sensitive in determining ablation threshold than the method based on the ablated spot diameter.

After determining the ablation parameters and analyzing the obtained surface properties, we tested using the scriber for preparing ITO electrodes with micrometer width. The approach is to use the laser to ablate closely aligned adjacent parallel lines and the remaining ITO film forms narrow ITO electrodes. The testing results on the three types of ITO-coated glass is shown in Fig. 8. The smallest ITO strip width obtained by this approach is less than 10 μm. The narrowest line of 5.1 μm was obtained on 5 Ω/□ slide (Fig. 8(a)、8(b)). The result demonstrated that micrometer ITO electrode could be quickly prepared using an inexpensive galvo scanner laser scriber. Such micro electrodes could be used as microsensor such as a flow sensor [2].

We further tested fabricating long ITO microwire using the ablation parameters for Fig. 8. The result is shown in Fig. 9 and Table 4. The wire with width of ~10 μm and length of 1000 μm has aspect ratio of 100. The expected wire resistances for 5 Ω/□, 50 Ω/□, and 90 Ω/□ are 500 Ω, 5 kΩ, and 9 kΩ, respectively. The deviations from the nominal values are 6%, 4%, and 2 %, respectively, which are not

significant. We conclude that the ablation process did not alter the resistivity of the ITO film.

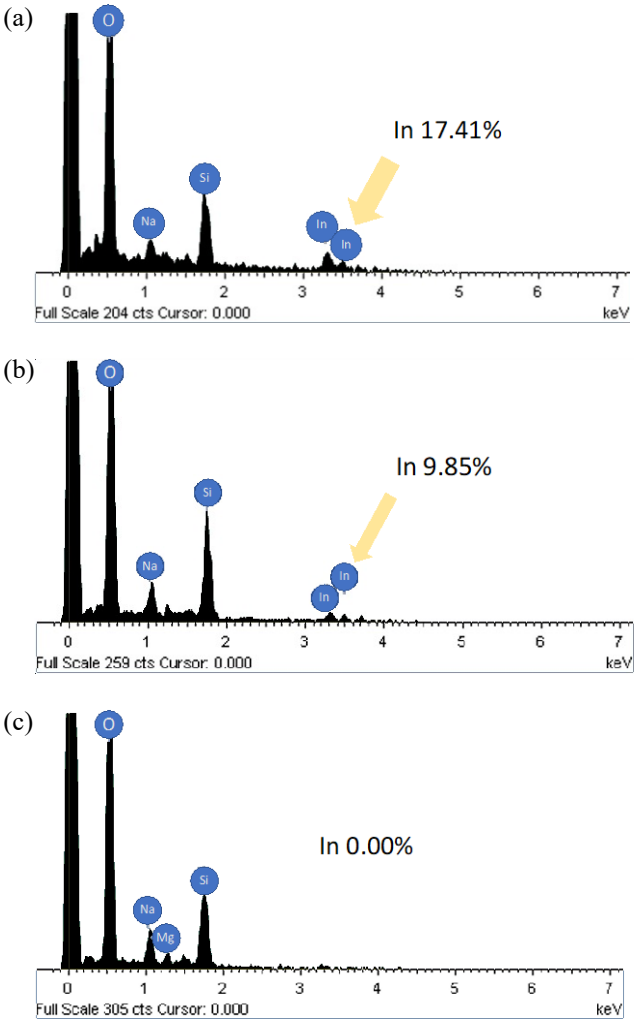

Fig. 7 The element distribution measured by EDS on 50 Ω/□ slide at the regions corresponding to those in Figures 6(c) and 6(d). (a) Pristine ITO slide surface. (b) Ablated region, fluence 4.3 J/cm^2. (c)Ablated region, fluence 5.5 J/cm^2. The measurement regions are marked in Figures 5(c) and 5(d).

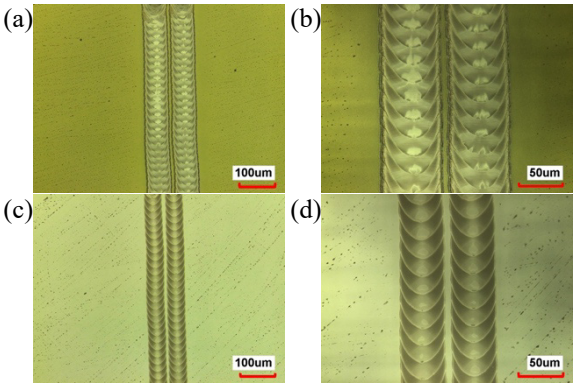

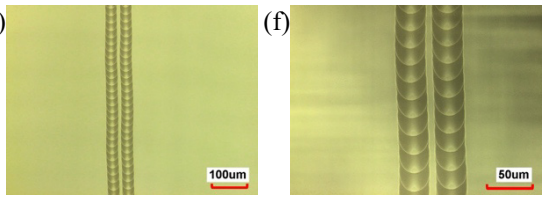

Fig. 8 Optical microscopic view of the micrometer ITO electrodes prepared by ablating two parallel lines. The scanning speed is 1000 mm/sec. (a) 5 Ω/□, 12.3 J/cm^2. (b) 5 Ω/□, 12.3 J/cm^2. (c) 50 Ω/□, 12.3 J/cm^2. (d) 50 Ω/□, 12.3 J/cm^2. (e) 90 Ω/□, 12.3 J/cm^2. (f) 90 Ω/□, 12.3 J/cm^2.

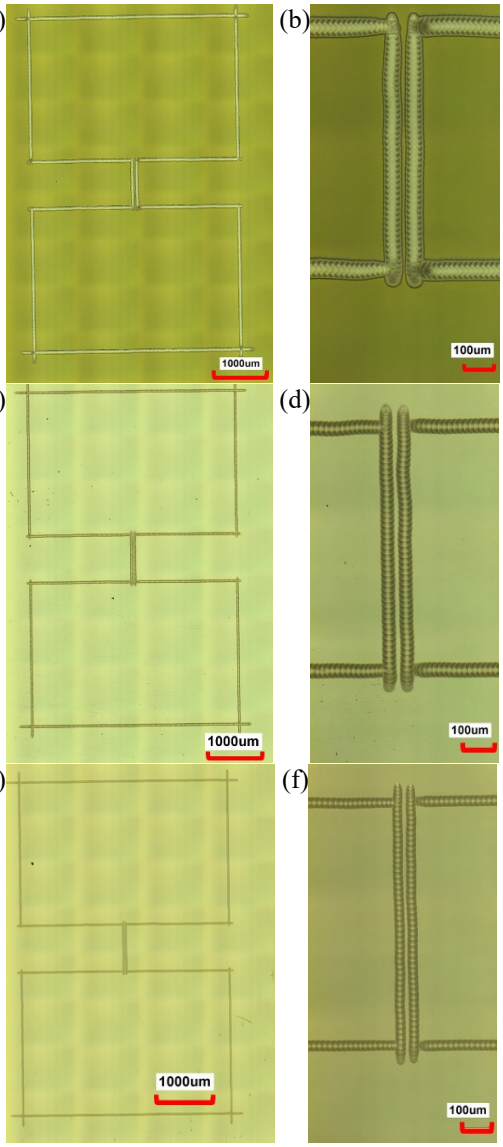

Fig. 9 Simple long microwires observed under VK9700 microscope. A pair of contacting pads at the top side and the down side of the microwire was for the connecting to testing probes of the multimeter. (a) 5 Ω/□, whole view. (b) 5 Ω/□, close-up. (c) 50 Ω/□, whole-view. (d) 50 Ω/□, close-up. (e) 90 Ω/□, whole-view. (f) 90 Ω/□, close-up.

Table 4 Resistance of the ITO microwires with a width of 10±4 μm and a length of 1000 μm on the three types of ITO-coated glass. The ablation fluences are the same as those used in Fig.8.

	5 Ω/□	**50** Ω/□	**90** Ω/□
resistance	471.3Ω	4.8KΩ	8.8KΩ

4. Conclusion

In this work, we presented a rapid method for determining ITO ablation threshold. The method relies on the conduction property of the ITO film. The resistance changes of an ITO test strip after the laser ablation can be rapidly measured and the lowest laser ablation fluence can be quickly determined. The method is simpler compared to the typical method that requires the microscopic measurement of laser ablated spot sizes. We determined the ITO laser ablation parameters for three types of ITO slides and prepared ITO conducting electrodes with width smaller than 10 μm. Several 10 μm wide ITO microwire with aspect ratio of 100 had been fabricated using this microfabrication platform. The ablation process did not alter the resistivity of the ITO film. This work demonstrated the effectiveness and flexibility of a modest and inexpensive NIR laser scriber.

Acknowledgments

The authors thank the partial financial support from National Science and Technology Council, Taiwan. (MOST 111-2113-M-001-046).

References

[1] Park, M., B.H. Chon, H.S. Kim, S.C. Jeoung, D. Kim, J.I. Lee, H.Y. Chu, and H.R. Kim: Opt. Laser. Eng., 44, (2006) 138.

[2] Cheng, J.-Y., M.-H. Yen, W.-C. Hsu, J.-H. Jhang, and T.-H. Young: J. Micromech. Microeng., 17, (2007) 2316.

[3] Alsaee, S.K., N.M. Ahmed, E. Mzwd, A.F. Omar, A.I. Aljameel, N. Afzal, I.A. Razak, and S. Arshad: Appl. Phys. B-Lasers. Opt., 128, (2022)

[4] Takai, M., D. Bollmann, and K. Haberger: Appl. Phys. Lett., 64, (1994) 2560.

[5] Rung, S., M. Rexhepi, C. Bischoff, and R. Hellmann: J. Laser. Micro. Nanoen., 8, (2013) 309.

[6] Tseng, S.F., W.T. Hsiao, K.C. Huang, D. Chiang, M.F. Chen, and C.P. Chou: Appl. Surf. Sci., 257, (2010) 1487.

[7] De Bonis, A., A. Galasso, V. Marotta, S. Orlando, A. Santagata, R. Teghil, S. Veronesi, P. Villani, and A. Giardini: Appl. Surf. Sci., 252, (2006) 4632.

[8] Ryuzo, T., T. Takaoka, H. Mizukami, T. Arai, and Y. Iwai: Proc. SPIE 2003,(2003) #4830.

[9] Yavas, O., C. Ochiai, and M. Takai: Appl. Phys. a-Mater., 69, (1999) S875.

[10] Munoz-Garcia, C., D. Canteli, S. Lauzurica, M. Morales, C. Molpeceres, E. Ros, P. Ortega, J.M. Lopez-Gonzalez, and C. Voz: Surf. Interfaces., 28, (2022)

[11] Kuang, Z., W. Perrie, D. Liu, P. Fitzsimons, S.P. Edwardson, E. Fearon, G. Dearden, and K.G. Watkins: Appl. Surf. Sci., 258, (2012) 7601.

[12] Raciukaitis, G., M. Brikas, M. Gedvilas, and G. Darcianovas: J. Laser. Micro. Nanoen., 2, (2007) 1.

[13] Cheng, C.W., I.M. Lee, W.C. Shen, C.Y. Lin, and J.S. Chen: J. Laser. Micro. Nanoen., 5, (2010) 213.

[14] Tanaka, R., T. Takaoka, H. Mizukami, T. Arai, and Y. Iwai: Proc. SPIE 2003, (2003) #5063.

[15] Cheng, C.W., J.S. Chen, and H.H. Chen: Mater. Manuf. Process., 25, (2010) 684.

[16] Lin, H.K., W.C. Hsu, and L.C. Tsao: Opt. Quant. Electron., 48, (2016)

[17] Dittrich, S., M. Spellauge, S. Barcikowski, H.P. Huber, and B. Gokce: Opto-Electron. Adv., 5, (2022)

[18] Lin, Z.Y., L.F. Ji, and M.H. Hong: Nano. Lett., 22, (2022) 7005.

[19] Sun, W.G., L.F. Ji, Z.Y. Lin, J.C. Zheng, Z.Y. Wang, L.T. Zhang, and T.Y. Yan: Adv. Funct. Mater., 32, (2022)

[20] Liu, J.M.: Opt. Lett., 7, (1982) 196.

[21] Xiao, S.Z., E.L. Gurevich, and A. Ostendorf: Appl. Phys. a-Mater., 107, (2012) 333.

[22] Stratan, A., A. Zorila, L. Rusen, and G. Nemes: Opt. Eng., 53, (2014)

[23] Choi, H.W., D.F. Farson, J. Bovatsek, A. Arai, and D. Ashkenasi: Appl. Opt., 46, (2007) 5792.

(Received: June 15, 2023, Accepted: July 29, 2023)